Applied Catalysis B: Environmental 147 (2014) 359–368

Contents lists available at ScienceDirect

Applied Catalysis B: Environmental

journal homepage: www.elsevier.com/locate/apcatb

Highly active Ni-promoted mesostructured silica nanoparticles for CO_2 methanation

M.A.A. Aziz[a], A.A. Jalil[a], S. Triwahyono[b,c,*], R.R. Mukti[d], Y.H. Taufiq-Yap[e], M.R. Sazegar[b]

[a] Institute of Hydrogen Economy, Faculty of Chemical Engineering, Universiti Teknologi Malaysia, 81310 UTM Johor Bahru, Johor, Malaysia
[b] Department of Chemistry, Faculty of Science, Universiti Teknologi Malaysia, 81310 UTM Johor Bahru, Johor, Malaysia
[c] Ibnu Sina Institute for Fundamental Science Studies, Universiti Teknologi Malaysia, 81310 UTM Johor Bahru, Johor, Malaysia
[d] Division of Inorganic and Physical Chemistry, Faculty of Mathematics and Natural Sciences, Institut Teknologi Bandung, Jl. Ganesha 10, Bandung 40132, Indonesia
[e] Catalysis Science and Technology Research Centre, Faculty of Science, Universiti Putra Malaysia, 43400 UPM Serdang, Selangor, Malaysia

ARTICLE INFO

Article history:
Received 17 April 2013
Received in revised form 29 August 2013
Accepted 17 September 2013
Available online 25 September 2013

Keywords:
CO_2 methanation
Ni/MSN
Basicity
Intra–inter particle pores
Oxygen vacancy

ABSTRACT

Mesostructured silica nanoparticles (MSN) and Ni loaded onto MSN (Ni/MSN) for the methanation of CO_2 were prepared by the sol–gel and impregnation methods. Catalytic testing was conducted in the temperature range of 423–723 K under atmospheric pressure in the presence of H_2. Ni supported on MSN was compared with others types of support such as MCM-41 (Mobile Crystalline Material), HY (protonated Y zeolite), SiO_2 and γ-Al_2O_3. The activity of CO_2 methanation followed the order: Ni/MSN > Ni/MCM-41 > Ni/HY > Ni/SiO_2 > Ni/γ-Al_2O_3. The nitrogen physisorption and pyrrole adsorbed IR spectroscopy results indicated that the high activity of Ni/MSN is due to the presence of both intra- and inter-particle porosity which led to the high concentration of basic sites. In addition, the correlation between N–H band intensity and the turnover frequency revealed that the methanation activity increased with increasing of the concentration of basic sites. The presence of defect sites or oxygen vacancies in MSN was responsible for the formation of surface carbon species, while Ni sites dissociated hydrogen to form atomic hydrogen. The surface carbon species then interacted with atomic hydrogen to form methane. The Ni/MSN catalyst performed with good stability and no deactivation up to 200 h.

1. Introduction

Recycling of CO_2 as a carbon source for chemicals and fuels should be considered as a more sustainable use of resources which may indeed lead to reduced consumption of carbon-based fossil resources without producing more CO_2 from the whole system. Thus, the catalytic conversion of CO_2 to fuels is a critical goal that should positively impact the global carbon balance by recycling CO_2 into usable fuels [1]. The CO_2 methanation reaction is called the Sabatier reaction and was first introduced by Sabatier and Senderens [2]. The methanation of carbon dioxide is an important catalytic process of fundamental academic interest with potential commercial applications [3]. Although interest in the large-scale manufacture of substitute natural gas from the products of coal gasification has greatly diminished in recent decades, carbon dioxide methanation, especially in the fuel cell and ammonia synthesis industry, can be used for the removal of trace CO from H_2-rich streams to prevent catalyst poisoning [4]. In addition, the National Aeronautics Space Administration (NASA) is also interested in applications of the Sabatier reaction for use in future manned space expeditions to Mars. Bringing terrene hydrogen to Mars will make it possible to convert the Martian carbon dioxide atmosphere into methane and water for fuel and astronaut life support systems [5].

Conversion of carbon oxides into methane with an acceptable reaction rate and selectivity are inherently difficult due to kinetic limitations, although they are exothermic and thermodynamically favorable. Therefore, catalysts, mostly Group VIII metals such as Ni [6–11], Ru [12,13], Rh [14–16], Pd [17,18] and Pt [19] supported on diverse porous materials, are usually required to achieve considerable methanation rates. Ni-based catalysts have been widely investigated for industrial purposes because nickel is inexpensive and readily available. Because the support has a significant influence on the morphology of the active phase, adsorption and catalytic properties [20], preparation of highly dispersed supported metal catalysts has been the focus of considerable research. Presently, various materials are used as the support for nickel catalysts such as γ-Al_2O_3 [6], MCM-41 [7], SBA-15 [8], ZrO_2 [9], CeO_2 [10] and zeolite [11]. High surface area supports are extensively used in industry for the preparation of metal catalysts. In the chemical processing industry, a catalyst with high activity, selectivity

* Corresponding author. Tel.: +60 7 5536076; fax: +60 7 5536080.
E-mail addresses: sugeng@utm.my, sugengtw@gmail.com (S. Triwahyono).

0926-3373/$ – see front matter © 2013 Elsevier B.V. All rights reserved.
http://dx.doi.org/10.1016/j.apcatb.2013.09.015

and stability is essential. To meet these requirements, the catalyst support should provide sufficient surface area and be composed of a robust material for high dispersion of the metal and stability. It has emerged that the support plays a very active role in the interaction between nickel and the support. Nickel compounds on different support surfaces result in a variable extent of what is generally called the "metal-support effect" [21–23]. This implies that catalysts with different characteristics exhibit variable performance in terms of activity and selectivity for a given process. One of the potential candidates for a new support for Ni catalysts is mesostructured silica nanoparticles (MSN). Previously, MSNs have been widely used in research such as in drug delivery [24,25], biomedical imaging [26,27] and catalysis [28,29]. This is due to their distinctive properties such as nanosize, ordered porous structure, extremely high surface area (>1000 m^2/g), large pore volume and well-defined and tunable pore size (1.5–10 nm). The pore diameters also can be tailored to host specific particles according to their dimensions [30]. These properties are necessary in sorption and catalysis applications, while maintaining the intrinsic properties of silica.

In the present approach, MSN was used as the support for a nickel-based catalyst for CO_2 methanation. It was expected that nickel particles would disperse well over the surface of the catalyst due to the large surface area and robustness of MSN. Therefore, the aim of the present work was the preparation of supported Ni catalysts and the characterization of their physicochemical properties, with emphasis on the clarification of the role of the support and the basicity of the catalyst. Additionally, the catalytic performance of these catalysts was investigated in CO_2 methanation. The probable mechanism of CO_2 methanation using Ni/MSN was also studied in detail. For comparison, we also studied different types of support such as MCM-41, SiO_2, γ-Al_2O_3 and HY.

2. Experimental

2.1. Catalyst preparation

MSN was prepared by the sol–gel method according to a report by Karim et al. [31]. The surfactant cetyltrimethylammonium bromide (CTAB; Merck), ethylene glycol (EG; Merck) and NH_4OH solution (QRec) were dissolved in water with the following molar composition of CTAB:EG:NH_4OH:H_2O = 0.0032:0.2:0.2:0.1. After vigorous stirring for about 30 min at 353 K, 1.2 mmol of tetraethyl orthosilicate (Merck) and 1 mmol of 3-aminopropyl triethoxysilane (Merck) were added to the clear mixture to give a white suspension solution. This solution was then stirred for another 2 h, and the samples were collected by centrifugation at 3000 rpm. The synthesized MSN were dried at 333 K and calcined at 823 K for 3 h to remove the surfactant.

MCM-41 was prepared based on a report by Beck et al. [32]. The solution of hexadecyltrimethylammonium bromide (Merck) was mixed with sodium silicate (Merck). After pH adjustment with 4 N HCl (QRec) to pH 11 and further stirring for 1 h, the gel was transferred to an autoclave for hydrothermal synthesis at 393 K for 96 h. The resultant solid was recovered by filtration, washed thoroughly with distilled water, dried at 313 K in a vacuum, and finally calcined at 823 K for 6 h.

The 5 wt% Ni loaded supports were prepared by the wet impregnation method over MSN, MCM-41, SiO_2 (Sigma-Aldrich), γ-Al_2O_3 (Sigma-Aldrich) and HY (Zeolyst) supports. The aqueous nickel nitrate ($Ni(NO_3)_2{\cdot}6H_2O$) (Merck, 99%) was impregnated on the support at 333 K, and was then dried in an oven at 383 K overnight before calcination in air at 823 K for 3 h.

2.2. Characterization

The crystalline structure of the catalyst was determined by X-ray diffraction (XRD) recorded on a powder diffractometer (Bruker Advance D8, 40 kV, 40 mA) using a Cu $K\alpha$ radiation source in the range of 2θ = 1.5–90°. The primary crystallite size of NiO (D_{NiO}) was calculated by means of the Scherrer equation [33]:

$$D_{NiO} = \frac{0.9\lambda}{B\cos\theta} \quad (1)$$

where λ is the X-ray wavelength corresponding to Cu-$K\alpha$ radiation (0.15406 nm), B is the broadening (in radians) of the nickel (2 0 0) reflection and θ is the angle of diffraction corresponding to peak broadening.

The BET analysis of the catalyst was determined by N_2 adsorption–desorption isotherms using a Quantachrome Autosorb-1 instrument. The catalyst was outgassed at 573 K for 3 h before being subjected to N_2 adsorption. The pore size distribution and pore volume were determined using the Barrett–Joyner–Halenda (BJH) method.

Pyrolle-FTIR spectroscopy was used to characterize the basic properties of catalyst [34,35]. Pyrrole is an amphoteric molecule which can either interact with the Lewis basic oxygen of silicate framework via the NH group by hydrogen bonding or with the Lewis acidic cation via the aromatic π-electrons interaction [35]. In the present work, pyrrole has been used as a probe molecule for the characterization of basic sites because it can be adsorbed reversibly due to its weak acidity. FTIR measurements were performed on an Agilent Cary 640 FTIR spectrometer equipped with a high-temperature stainless steel cell with CaF_2 windows. A sample of 30 mg in the form of a self-supported wafer was reduced in H_2 stream (100 ml/min) at a rate of 5 K/min to 773 K for 4 h and cooling to room temperature under He atmosphere. Then, the reduced catalyst was exposed to 2 Torr of pyrrole at room temperature for 30 min, followed by outgassing at four different temperatures of 303, 323, 373 and 423 K for 30 min, respectively. All spectra were recorded at room temperature with a spectral resolution of 5 cm^{-1} with five scans.

H_2 chemisorption measurements were carried out on Quantachrome Autosorb-1 at 293 K. Approximately 200 mg of catalyst was reduced in H_2 stream (100 ml/min) at 773 K for 4 h, followed by outgassing at 773 K for 2 h. Then, the catalyst was cooled down to 293 K for the H_2 chemisorption measurement. The H_2 monolayer uptake of the catalysts was calculated by extrapolating the H_2 adsorption isotherm to zero pressure. Assuming that Ni^{2+} ions were reduced completely and the Ni particles were spherical. The number of nickel atom on the surface was calculated when the hydrogen atom reached H/Ni_s ratio of unity. The percent Ni dispersion is calculated by dividing the number of exposed surface Ni atoms by the total amount of Ni in the catalyst. The nickel surface area were calculated by assuming that the cross-sectional area of atomic nickel is 6.49×10^{-20} m^2/Ni-atom.

A JEOL JES-FA100 ESR spectrometer was used to observe the formation of electron holes or unpaired electrons after in vacuo heating and to observe the interaction of the electron holes or unpaired electrons with carbon dioxide and electrons formed from molecular hydrogen at room temperature to 473 K. The catalyst was reduced in H_2 stream (100 ml/min) at 773 K for 4 h, followed by cooling down in He atmosphere to adsorption temperature. Then the catalyst was exposed to 4 Torr of carbon dioxide at room temperature, followed by stepwise heating from 323 to 473 K in 50 K increments. The carbon dioxide pre-adsorbed sample was then exposed to 16 Torr hydrogen and heated stepwise from 323 to 473 K in 50 K increments.

Coke deposits on the catalysts were characterized with a Mettler Toledo TGA/SDTA 851e instrument. The catalyst (~12 mg) was

heated under nitrogen stream up to 1150 K. The temperature ramp of 10 K/min was applied and the catalysts weight as a function of temperature were monitored.

2.3. Catalytic performance

Carbon dioxide methanation was conducted in a fixed-bed quartz reactor with an interior diameter of 8 mm at atmospheric pressure and in a temperature range of 423–723 K. The thermocouple was directly inserted into the catalyst bed to measure the actual pretreatment and reaction temperatures. The catalyst was sieved and selected in the 20–40 μm fraction. Initially, 200 mg of catalyst were treated in an oxygen stream (F_{oxygen} = 100 ml/min) for 1 h followed by a hydrogen stream ($F_{hydrogen}$ = 100 ml/min) for 4 h at 773 K and cooled down to the desired reaction temperature in a hydrogen stream. When the temperature became stable, a mixture of H_2 and CO_2 was fed into the reactor at a specific gas hourly space velocity (GHSV) and H_2/CO_2 mass ratio. All gases were controlled by calibrated mass flow controllers (SEC-400 MK2, Stec Ltd., Japan). Four kinds of experiments were then performed: (i) the CH_4 formation rate (activity) was measured in the temperature range of 423 to 723 K: The activity was monitored with decreasing temperature and back to verify stable catalyst conditions during these measurements, (ii) the effect of H_2/CO_2 mass ratios ranging from 1 to 8 were determined, (iii) the GHSV was varied from 10,000 to 70,000 ml/g h with mass of the catalyst, m_{cat} = 200 mg and (iv) stability testing was carried out for 200 h at 573 K. The composition of the outlet gases was analyzed by an on-line 6090 N Agilent gas chromatograph equipped with a GS-Carbon PLOT column and a TCD detector. The lines from the outlet of the reactor to the GC were heated at 383 K to avoid condensation of the products. To determine the activity and selectivity, the products were collected after 1 h of steady-state operation at each temperature. The conversion of carbon dioxide and selectivity were calculated by the following equations:

$$X_{CO_2}(\%) = \frac{F_{CO_2,in} - F_{CO_2,out}}{F_{CO_2,in}} \times (100\%) \quad (2)$$

$$S_x(\%) = \frac{F_{x,out}}{F_{CO_2,in} - F_{CO_2,out}} \times (100\%) \quad (3)$$

where X_{CO_2} is the conversion of carbon dioxide (%), S_x is the selectivity (%), x = CH_4 or CO, F is a molar flow rate of CO_2 or product in mole per second. The CH_4 formation rate was reported as moles of CH_4 produced per mole of Ni_{total} per second. The turnover frequency (TOF) was calculated as moles of CH_4 produced per mole of $Ni_{surface}$ per second.

3. Results and discussion

3.1. Physical properties of catalysts

Fig. 1A shows the small-angle XRD patterns for the MSN, Ni/MSN and Ni/MCM-41 catalysts. The patterns show three peaks, indexed as (1 0 0), (1 1 0) and (2 0 0), which are reflections of the typical two dimensional hexagonally ordered mesostructure (*p6mm*), demonstrating the high quality of mesopore packing. The ordered MSN support structure was not disturbed by the inclusion of Ni. No shifts in the peaks of the small-angle XRD patterns were observed, but the intensities decreased slightly with the introduction of Ni, indicating minor structural degradation of MSN. As evaluated from the intensities of *p6mm*, the (1 0 0) peak in the XRD patterns, Ni/MCM-41 had greater pore order than Ni/MSN. The presence of metal crystallites of NiO supported on various supports were characterized using wide-angle XRD (30–90°), as shown in Fig. 1B. For all

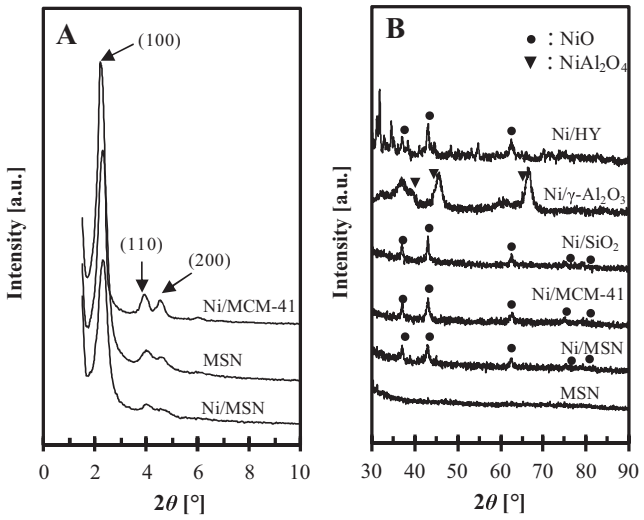

Fig. 1. Small-angle (A) and wide-angle (B) XRD patterns of MSN- and Ni-based catalysts.

catalysts (except Ni/γ-Al_2O_3), the diffraction peaks at 37.3°, 43.2°, 62.9°, 75.3° and 79.4° were attributed to a face-centered cubic crystalline NiO [36]. No NiO crystals were observed for Ni/γ-Al_2O_3, which may have been due to the superposition of NiO with γ-Al_2O_3 peaks; additionally, the crystal size of NiO particles may have been too small and beyond the detection limit of XRD. However, distinct peaks of $NiAl_2O_4$ were observed at 37.0°, 45.0° and 65.5° [37]. The average crystal diameter of NiO was estimated from the main peak marked from its indices (2 0 0) plane using the Scherrer equation. As shown in Table 1, the average crystal size of NiO (D_{NiO}) gradually increased from 9.9 to 19.8 nm, following the order Ni/MSN < Ni/MCM–41 < Ni/SiO_2 < Ni/HY. The discrepancies in NiO crystal size among the catalysts were mainly due to the surface area of the support material. Similar results have been reported by Wang and Lu [38], in which the Ni particle size on SiO_2 and α-Al_2O_3 also varied, depending on the support's porosity. Supports with a more porous structure or, on the other hand, a high surface area, lead to smaller nickel particle sizes.

Nitrogen adsorption-desorption isotherms and corresponding pore size distribution plots of all catalysts are shown in Fig. 2. For MSN-type catalysts (MSN and Ni/MSN) (Fig. 2A and B), all isotherms showed a type IV profile and type H1 hysteresis loops (IUPAC classification), characteristic of mesoporous materials with highly uniform cylindrical pores. Moreover, these MSNs showed two steps of capillary condensation with the first step at P/P_o = 0.3 due to mesopores inside the MSN (intraparticles). Secondly, at higher partial pressure (P/P_o = 0.9), a small hysteresis loop was observed for both MSN and Ni/MSN, which was attributed to interparticle textural porosity, which indirectly reflects the size of particles, i.e. a higher partial pressure was associated with a smaller particle size [39,40]. The slope of the first hysteresis loop decreased by 37% after the introduction of Ni, while the slope of the second hysteresis loop was nearly unchanged. However, the relative pressure for Ni/MSN shifted slightly to a higher pressure, indicating that the particle size of Ni/MSNs was smaller than those of MSN. Ni/MSN retained the same shape of the isotherm as observed for MSN; however, the amount of adsorbed nitrogen decreased by 18% after the introduction of Ni. The pore size distribution for both catalysts was quite narrow and monomodal, showing a peak pore diameter at 2.8 and 3.4 nm with a peak width of ca. 4 and 6 nm at half-maximum for MSN and Ni/MSN, respectively. A similar pattern was reported by Cauda et al., who observed the presence of intra- and inter-particle porosity on mesoporous silica nanoparticles [41].

Table 1
Physical properties of the catalysts. All modified catalysts were loaded with 5 wt% Ni.

Catalyst	BET surface area (m^2/g)[a]	Pore volume (cm^3/g)[b]	Pore size (nm)[b]	D_{NiO}[c] (nm)	Ni dispersion (%)[d]	Ni surface area (m^2/g)[d]
MSN	1051	0.758	2.8	–	–	–
Ni/MSN	879	0.798	3.4	9.9	11.9	40.9
Ni/MCM-41	857	0.609	2.7	10.5	10.7	36.7
Ni/HY	629	0.250	5.8	19.8	8.2	28.0
Ni/SiO_2	210	0.767	10	17.8	7.1	24.2
Ni/γ-Al_2O_3	158	0.644	13.2	–	6.3	21.4

[a] Obtained from BET method.
[b] Obtained from BJH desorption average pore volume and pore diameter.
[c] Determined by XRD (Debye–Sherrer method).
[d] Determined by hydrogen chemisorption.

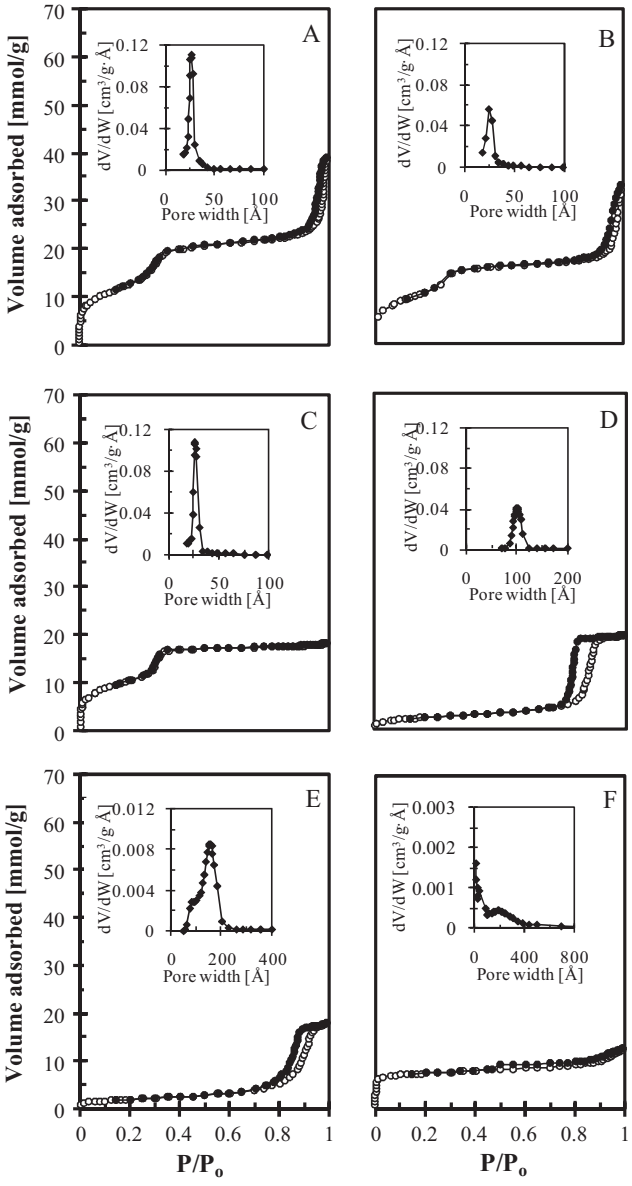

Fig. 2. N_2 adsorption–desorption isotherm of (A) MSN, (B) Ni/MSN, (C) Ni/MCM-41, (D) Ni/SiO_2, (E) Ni/γ-Al_2O_3 and (F) Ni/HY. The inset shows the pore size distribution.

For the Ni/MCM-41 catalyst (Fig. 2C), the adsorption isotherms were designated as Type IV (IUPAC classification). The sample presented a clear and sharp adsorption step at relative pressure values ($P/P_o = 0.3$) due to the capillary condensation of N_2 inside intraparticle pores. In contrast to the MSN-type catalysts, the Ni/MCM-41 catalyst in our study had no interparticle pores located at about $P/P_o = 0.9$. The adsorption branches of all nitrogen isotherms were completely superimposed on the desorption ones, indicating reversible pore filling and emptying. One of the important features of MCM-41 mesoporous silica is that their adsorption isotherms rise steeply within a very narrow pressure range, suggesting a uniform pore size [42]. The pore size distribution in our Ni/MCM-41 catalyst was quite narrow and monomodal, showing a peak pore diameter at 2.7 nm with a peak width of ca. 4 nm at half-maximum.

The isotherm for the Ni/SiO_2 catalyst also corresponded to type IV (Fig. 2D). The appearance of a type H1 hysteresis loop (P/P_o range of 0.55–0.8) may indicate, in this case, that the mesoporous material consisted of agglomerates of approximately spherical particles of fairly uniform size and distribution [43]. The pore size distribution in the Ni/SiO_2 catalyst was also monomodal, showing a peak pore diameter at 10 nm, and was quite narrow, although much broader than that of Ni/MSN and Ni/MCM-41 as the peak width at half-maximum was ca. 21 nm. A similar isotherm was observed on a Co–SiO_2/sol–gel which showed a type IV isotherm and an H1 type hysteresis loop. The authors are also mentioned a monomodal pore size distribution and larger pore size than the Co-MCM-41 catalyst [44].

The isotherms of Ni/γ-Al_2O_3 (Fig. 2E) tended to reach a plateau above a certain relative pressure, indicating that most of the pores in these solids fell within the mesopore range. The hysteresis loops of this catalyst can be classified as type H2 according to the IUPAC recommendations for gas physisorption data analysis [45], and suggest the presence of nearly tubular mesopores with a relatively narrow pore size distribution. The nitrogen isotherms of the Ni/HY sample are shown in Fig. 2F. The sample had a type I isotherm, characteristic of purely microporous materials. The irreversibility of the isotherm at very high relative pressure ($P/P_o > 0.9$) could be assigned to the adsorption of nitrogen in interparticle pores generated by the agglomeration of zeolite crystals.

Table 1 summarizes the textural properties of all samples. The BET surface area of MSN and Ni/γ-Al_2O_3 showed a descending trend from 1051 to 158 m^2/g with increased mean pore diameter from 2.8 to 13.2 nm, evidencing the inverse relationship between pore size and surface area typical of inorganic porous oxides with conventional morphologies (i.e. intraparticle porosity). Surface area of MSN was 1051 m^2/g, which was slightly higher than that of conventional MCM-41 (941 m^2/g). The decrease in the amount of absorbed nitrogen on the Ni/MSN catalyst was due to a reduction in the surface area and loading of Ni, which has a much higher density than silica. Also, the decrease in the BET surface area provides complementary evidence of pores being blocked by nickel oxide nanoparticles. The high surface area of the support promotes high dispersion of the metal on the surface of the catalyst. However, the pore size of MSN was slightly increased from 2.8 to 3.4 nm after the

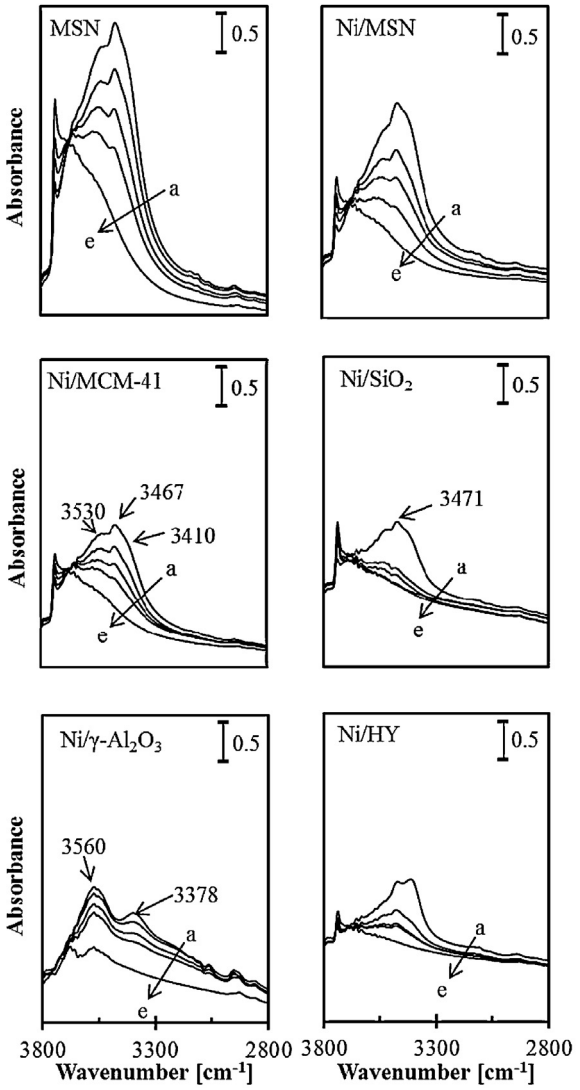

Fig. 3. IR spectra of pyrrole adsorbed on reduced catalysts, exposed to 2 Torr pyrrole at 303 K, followed by outgassing at (a) 303 K, (b) 323 K, (c) 373 K and (d) 423 K; (e) shows the spectra before adsorption.

introduction of Ni. This alteration of the pore size was due to the isomorphous substitution of nickel atoms into silica frameworks which leads to significant contraction of walls and consequently, expansion of pores. Similar phenomenon was also observed on Rh loaded on alumina [15] and Ni loaded on KIT-6 (a kind of mesoporous silica) [36]. In contrast, the size of NiO on MSN determined by XRD was larger than the average pore size of MSN. Therefore, in the present study, it is suggested that the location of NiO is both inside the pore mouth and on the surface of MSN. However, the location of NiO may not be important in a methanation study. Lu and Kawamoto [8] reported that the methanation of CO_2 by NiO/SBA-15 was not affected by the location of NiO, whether on the outer surface or inside the SBA-15 pores. The dispersion of Ni on the support is correlated well to the BET surface area in which high surface area of MSN exhibited high dispersion of Ni.

3.2. Basic properties of the catalysts

The IR spectra of pyrrole adsorbed on Ni loaded on the support catalysts in the N-H stretching region are shown in Fig. 3. For all catalysts, the main broad band situated at about 3475–3200 cm^{-1} can be assigned to the N–H stretching vibrations of chemisorbed

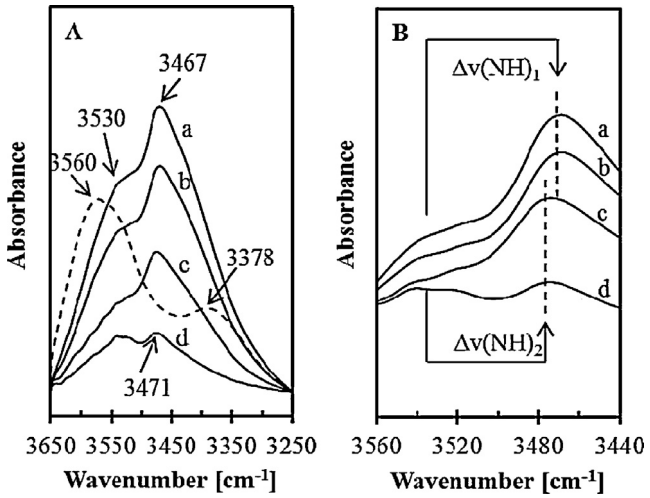

Fig. 4. Normalized IR spectra of pyrrole adsorbed on reduced catalysts after outgassing at 423 K for the catalysts (a) Ni/MSN, (b) Ni/MCM-41, (c) Ni/HY and (d) Ni/SiO_2. The dotted line represents $Ni/\gamma\text{-}Al_2O_3$.

pyrrole (C_4H_4NH) interacting with the basic sites of framework oxygens. The H-donor pyrrole properties allowed the formation of C_4H_4NH–O bridges with basic oxygen. In the cases of MSN, Ni/MSN and Ni/MCM-41, the band at 3530 cm^{-1} indicates the position of a pyrrole N–H band in the gas phase [46] and the band at 3410 cm^{-1} indicates the physisorbed pyrrole in a liquid-like state [47], where the N–H group interacts with the π-system of another pyrrole molecule. The band at 3467 cm^{-1} is attributed to the perturbed N–H stretch of pyrrole molecules interacting with the surface. Similar features were observed upon increasing the outgassing temperature from 303 to 423 K. The narrow band at 3733 cm^{-1}, indicating isolated SiOH species increased and a broader absorption band at about 3530 cm^{-1} due to H-bonded SiOH interacting with the pyrrole N–H band in the gas phase increased significantly.

A similar pattern was observed for the Ni/SiO_2 sample. The band at 3471 cm^{-1} was assigned to the pyrrole species forming intermolecular bonds. However, the band was largely removed upon evacuation at room temperature due to the weak interaction of the pyrrole species with SiO_2. This observation is in agreement with Scokart and Rouxhet [48], who observed the weak adsorption of pyrrole on SiO_2 at around 3410–3420 cm^{-1}. For the $Ni/\gamma\text{-}Al_2O_3$ catalyst, the band at 3560 cm^{-1} is attributed to surface hydroxyls interacting with pyrrole. The band appearing at 3378 cm^{-1} [49] is due to N–H vibration of adsorbed species forming intermolecular bonds. According to the figure, the former band is stronger than the latter. This is due to the desorption rate of the 3560 cm^{-1} band, which is much lower than the band at 3378 cm^{-1}. The band at 3560 cm^{-1} remained up to desorption at 423 K, while the band at 3390 cm^{-1} diminished. For the Ni/HY catalyst, the proton of the –NH group interacted with the framework basic oxygen atoms, forming hydrogen bridges (C_4H_4NH–O_{zeol}). The main bands were similar to the MSN-type catalyst and were observed at 3530 and 3467 cm^{-1}.

The basic sites of the catalysts can be determined based on the intensity of the main peaks at 3467 cm^{-1} (Ni/MSN and Ni/MCM-41), 3471 cm^{-1} (Ni/HY and Ni/SiO_2) and 3378 cm^{-1} ($Ni/\gamma\text{-}Al_2O_3$). The normalization spectra for the samples are presented in Fig. 4A. High intensity indicates a high concentration of basic sites possessed by the catalyst. Thus, the number of basic sites of Ni catalysts decreased following the sequence Ni/MSN > Ni/MCM-41 > Ni/HY > $Ni/\gamma\text{-}Al_2O_3$ > Ni/SiO_2. It is worth mentioning that the Ni/MSN catalysts showed fewer available sites for the adsorption of pyrrole than the MSN support. This result shows that Ni blocks

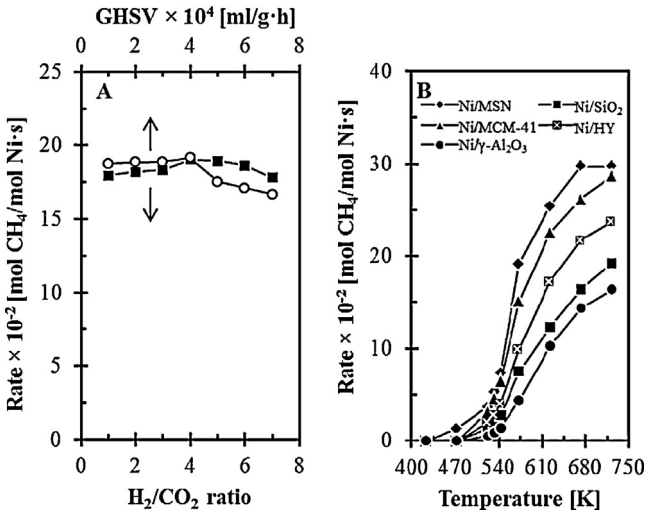

Fig. 5. (A) Dependence of the activity on the H_2:CO_2 mass ratio and GHSV at a temperature of 573 K. (B) Activity of all catalysts at the steady state as a function of the reaction temperature at GHSV = 50,000 ml/g h and H_2/CO_2 = 4:1.

some of the pyrrole adsorption sites of the support, and this led to a decrease in CO_2 adsorption on the Ni/MSN catalyst. On the other hand, increasing the basicity of the catalyst can improve its CO_2 adsorption ability. Recently, da Silva et al. [50] studied the effect of Ni on SiO_2 and ZrO_2 using TPD of CO_2. Both ZrO_2 and Ni/ZrO_2 are able to adsorb CO_2. However, it was verified that the Ni/ZrO_2 catalyst shows fewer available sites for the adsorption of CO_2 than the ZrO_2 support. This result shows that Ni blocks some of the CO_2adsorption sites of the support. Similarly, SiO_2 adsorbs small amounts of CO_2 and the Ni/SiO_2 catalyst adsorbs even less than SiO_2. This result indicates that SiO_2 interacts weakly with CO_2 and that the presence of Ni further reduces this adsorption.

Pyrrole is also used for measuring the strength of basic sites [51]. The IR band ascribed to N–H stretching vibrations shifted to a lower wavenumber upon the interaction of the H atom in pyrrole with a basic site. The negative charge is closely associated with the strength of the basic site. Ni/γ-Al_2O_3 was excluded from the analysis due to differences in the structure and the N–H stretching band. As depicted in Fig. 4B, the N–H stretching vibration shifted with respect to the N–H band in the gas phase (3530 cm^{-1}) for Ni/MSN and Ni/MCM-41; $\Delta\nu(NH)_1 = -63\ cm^{-1}$ for Ni/HY and $\Delta\nu(NH)_2 = -59\ cm^{-1}$ for Ni/SiO_2. Therefore, it is suggested that the basic strengths of the Ni catalysts are in the order Ni/MSN ≈ Ni/MCM-41 > Ni/HY ≈ Ni/SiO_2.

3.3. Catalytic performance

3.3.1. Influence of H_2:CO_2 mass ratio and GHSV

Fig. 5A shows the influence of the H_2:CO_2 mass ratio and GHSV on the catalytic performance of Ni/MSN for the methanation reaction. The activity of the catalyst showed a volcano-shaped trend with respect to the mass ratio of H_2:CO_2. Increasing the H_2:CO_2 ratio produced a positive effect on the activity up to H_2:CO_2 = 4:1 and slightly decreased up to H_2:CO_2 = 7:1. The increase and decrease of the catalytic activity on the effect of H_2:CO_2 ratio may be due to the change of the amount of molecular hydrogen in the reaction stream. The optimum ratio of H_2:CO_2 = 4:1 has a suitable amount of molecular hydrogen in which the adsorbed hydrogen on the catalyst simultaneously hydrogenating the carbonate species on the surface of the catalyst. However, our results conflict with those of Solymosi [52], who found very little influence of the H_2:CO_2 ratio on the selectivity of Rh catalysts. It is important to note that many studies focus on the methanation of CO_2 under conditions relevant for methane formation, at stoichiometric conditions (H_2:CO_2 = 4:1) [7,9,53]. Only a few studies deal with reaction atmospheres with a high excess of hydrogen (H_2:CO_2 = 15:1–125:1) [6,8]. The different reactant ratios may have considerable effects on the reaction behavior and the dominance of a specific reaction pathway. In this sense, studies performed at close stoichiometric H_2:CO_2 ratios may lead to mechanistic conclusions that are not necessarily relevant for the reaction under conditions typical for the selective methanation in H_2-rich reformate gases. The activity also increased with an increase in GHSV up to 50,000 ml/g h and slowly decreased to 70,000 ml/g h. Hence, it can be concluded that the Ni/MSN catalyst layers prepared in this work show adequate activity to catalyze the methanation reaction in micro-channel reactors.

3.3.2. Correlations between properties and catalytic performance

The influence of the reaction temperature was assessed at 423–723 K with GHSV = 50,000 ml/g h and H_2:CO_2 = 4:1 as depicted in Fig. 5B. Under these conditions, the support alone was totally inactive for CH_4 production, and all catalysts (except Ni/MSN) started being active at 523 K. This indicated that metallic nickel is necessary for CO_2 methanation over the studied catalytic system. The activity of all Ni catalysts showed an obvious increase with increasing temperature. When the reaction temperature was increased to 623 K, the rate of reaction reached 0.25 mol CH_4/mol Ni s which nearly three times greater than that of 573 K. The TOF at temperature of 573 K is 1.61 s^{-1} and this value is the highest yet reported comparison with the previous report [54]. Recently, Lu and Kawamoto have reported that 70%NiO/SBA-15 showed high catalytic activity for CO_2 methanation with CO_2 conversion and CH_4 selectivity of 89.4% and 100%, respectively, at 450 °C and H_2:CO_2 = 4:1 [8]. Accordingly, Ni/MSN developed in the present study also had an excellent activity for CO_2 methanation at much lower concentration of Ni (5 wt%). The rate of reaction was slightly maintained with the further temperature increase to 723 K in which the conversion was reached 100% conversion. From this observation, it can be deduced that on this condition, most of the CO_2 has been converted to CO, thus allowing the methanation of CO_2 at high temperature since methanation of CO_2 dominates at higher temperatures [55].

At reaction temperature of 573 K, the sequence of catalytic activity is as follows: Ni/MSN > Ni/MCM-41 > Ni/HY > Ni/SiO_2 > Ni/γ-Al_2O_3. The Ni/MSN catalyst exhibited the highest activity even at low temperatures (573 K). As presented in Table 2, the major products were always methane with a small amount of carbon monoxide; no C_2 or heavier hydrocarbons were observed in our experiments. At similar conversion level $\left(X_{CO_2} = 50\%\right)$, the selectivity for CH_4 and CO for all Ni catalysts were maintained at >95 and <5%, respectively. However, Ni/MSN showed the highest selectivity for CH_4 (99.9%), followed by Ni/MCM-41, Ni/SiO_2, Ni/HY and Ni/γ-Al_2O_3. Generally, hydrogenation of CO_2 is known to produce CH_4 with much higher selectivity than that of CO [56] since the reaction is believed to proceed through the hydrogenation of surface carbon species, C(a), formed by dissociation of strongly adsorbed CO. Thus, it has been suggested that the higher selectivity of CO_2 hydrogenation to methane is due to a lower amount of C(a) species present in this reaction [56,57] and/or due to the presence of lower amounts of weakly adsorbed CO, which retards hydrogenation of surface carbon species. Thus, it can be concluded that the Ni/MSN and Ni/γ-Al_2O_3 has the highest and the lowest amount of C(a) species on the surface of the catalyst. The apparent activation energies (E_a) of the activity for all Ni catalysts were studied in the range of 523–573 K. The E_a values increased in the order Ni/MSN < Ni/MCM-41 < Ni/HY < Ni/SiO_2 < Ni/γ-Al_2O_3. Comparable values for the E_a were reported by Inui and Funabiki [58] and Van Herwijnen et al. [59] for this reaction in a H_2/CO_2 mixture on Ni/SiO_2 (82 kJ/mol) and Ni/γ-Al_2O_3 (106 kJ/mol) catalysts, respectively.

Table 2
Catalytic testing results of CO_2 methanation.

Catalyst	Rate[a] × 10^{-2} (mol CH_4/mol Ni_{total} s)	TOF[a] (s^{-1})	[a] (%)	Selectivity[b] (%)		E_a[c] (kJ/mol)	Coke content (%)[d]
				CH_4	CO		
MSN	–	–	0.4	0	100	–	–
Ni/MSN	19.16	1.61	64.1	99.9	0.1	76	0.0
Ni/MCM-41	15.12	1.41	56.5	98.3	1.7	78	0.8
Ni/HY	9.90	1.21	48.5	96.4	3.6	81	4.7
Ni/SiO_2	7.51	1.06	42.4	96.6	3.4	84	7.5
Ni/γ-Al_2O_3	4.36	0.69	27.6	95.2	4.8	103	9.1

[a] Reaction condition: T = 573 K, H_2/CO_2 = 4/1, GHSV = 50,000 ml/g-cat h.
[b] At similar conversion level, for all catalysts.
[c] E_a values were determined in the range of 523–573 K.
[d] Determined from TGA analysis. Calculated as (g of deposits)/(g of calcined sample) × 100%.

The high activity of Ni/MSN may be due to the existence of both intra- and inter-particle porosity and the high basicity of the catalysts and this led to the high Ni dispersion on the surface of MSN. This property contributes to the high surface area and thus increases the active sites (Ni) of the catalyst. The interparticle pores could facilitate the transport of the reactants H_2 and CO_2 and product molecules during the catalytic reaction, making Ni/MSN more accessible for CO_2 methanation, and thus allowing higher CO_2 conversion to be obtained. Wang et al. reported the role of interparticle pores in Au/MCM, which increased the activity in terms of CO conversion [60]. Khitev et al. studied the skeletal isomerization of 1-butene over micro/mesoporous materials based on FER zeolite. They reported that interparticle pores or intercrystalline ordered mesopores improved the accessibility of the acid sites and the creation of new pore openings [61].

Diffusion limitation on catalytic reaction is significant when the molecular size of the reactant is close to the pore size. Molecules with a large molecular size experience large amounts of high restriction due to hydrodynamic drag and steric hindrance [62]. Diffusion limitation of reactants to catalytic reaction is negligible when the rate of the surface reaction is sufficiently slow. On the other hand, the diffusion limitation is predominant on metal catalysts supported on porous materials, when rates of collisions of reactant molecules with the pore wall are higher than those of intermolecular collisions. To determine if the internal diffusion limited the overall CO_2 methanation rate under our reaction conditions, the Weisz–Prater criterion [63] was applied as given by,

$$N_{WP} = \frac{\Re R_P^2}{C_s D_{eff}} < 1 \quad (4)$$

where $\Re$ is the reaction rate of CO_2 per unit volume of the catalyst $\left(\Re = 3.92 \times 10^{-9}\ \text{mol/cm}^3\ \text{s}\right)$, R_p is the particle radius of catalyst (0.021 cm), C_s is the surface concentration of CO_2 and D_{eff} is the pore diffusion. Since the mass transfer in the surface around the particle was a fast step, we assumed that the surface concentration of CO_2 (C_s) in the external surface of the particle, was equal to the concentration of CO_2 in the bulk. Thus, by taking $C_s = P_{CO_2}/RT$, the calculated value of C_s is 5.32×10^{-6} mol/cm^3. The Ni catalysts has pore diameter of 3.4 nm, which is much less than 100 nm; consequently, pore diffusion will be dominated by Knudsen diffusion and $D_{eff} \approx D_{Kn} = 1/3vd$, where v is the average molecular velocity (5.25×10^4 cm/s) and d is the average pore diameter (3.4×10^{-9} m). If $N_{WP} \leq 1$, limitation in internal mass transfer is negligibly low and consequently no concentration gradient exists within the pore, whereas if $N_{WP} \geq 1$, the resistance to pore diffusion severely limits the reaction. Under the reaction conditions (P = 1 atm, T = 573 K), the value of N_{WP} for Ni/MSN for CO_2 were calculated to be 2.61×10^{-4}. The result showed that the influence of internal mass-transfer limitations was indicated to be negligible. The numbers of N_{WP} were also not satisfied for the others types of catalysts studied.

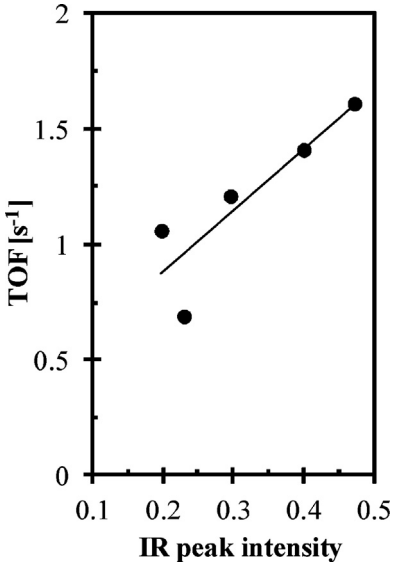

Fig. 6. Variations in the FTIR signal intensities with TOF. IR peak intensity was taken at 3467 cm^{-1} for (Ni/MSN and Ni/MCM-41) and 3471 cm^{-1} for (Ni/HY and Ni/SiO_2).

The presence of a high concentration of basic sites on Ni/MSN also contributed to the high activity. As shown in Fig. 6, there was a good correlation between TOF and the IR peak intensity of N–H stretching of each Ni catalysts. On the other hand, the TOF increased with an increase in the concentration of basic sites. This is clearly indicates that a large amount of basic sites on the catalyst support is crucial for high adsorption of CO_2 onto the support. It was, therefore, concluded that the nickel supported on MSN was more active than others supports in the present study.

Although the reaction pathways and mechanisms of the hydrogenation of CO_2 to CH_4 as well as the active surface species are still under debate, it is accepted that CO_2 adsorbed on the support reacts with the dissociated hydrogen from metal sites to produce CH_4 [12,17]. In this study, the probable mechanism of CO_2 methanation over the Ni/MSN catalyst was determined by electron spin resonance (ESR) studies. In general, ESR spectroscopy is a technique for studying materials with unpaired electrons. In the present work, this technique is complementarily used to study the occurrence of oxygen vacancies in MSN, whereby the technique were also done to detect the oxygen vacancies on SBA-15 [64], SnO_2 [65] and TiO_2 [66]. Albeit this characterization technique claimed to be sensitive to oxygen vacancies, it led to quite controversial assignments of the spectra, however, many ESR studies attribute the commonly observed signal g = 1.99 to the presence of electrons trapped in oxygen vacancies [65,67–69]. Furthermore, the change in ESR signal intensity give a simultaneous evidences of changing in oxygen vacancies [65]. As shown in Fig. 7, the generation of radical sites on

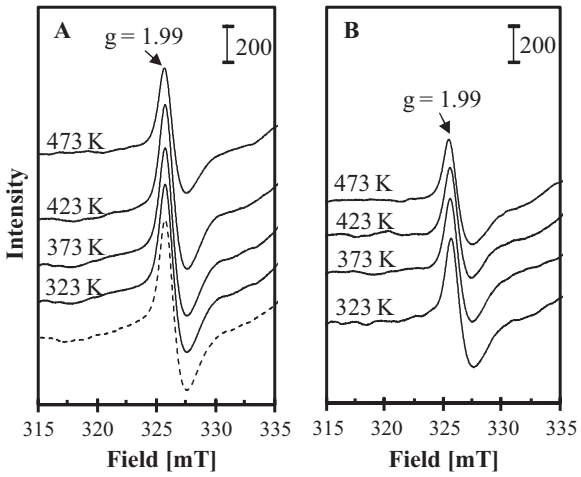

Fig. 7. (A) ESR signals of reduced Ni/MSN after heating in the presence of 4 Torr carbon dioxide from 323 to 473 K. (B) ESR signal of the carbon dioxide preadsorbed sample heated in 16 Torr hydrogen from 323 to 473 K. The dotted line represents Ni/MSN after reduced at 673 K.

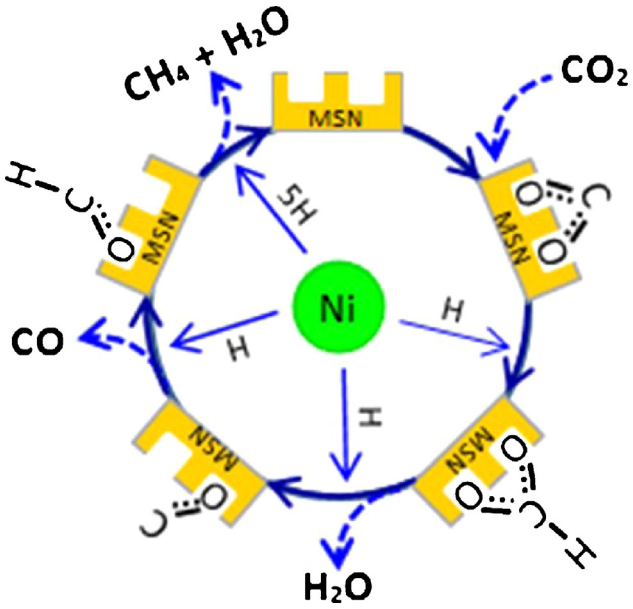

Fig. 8. A probable mechanism for Ni/MSN whereby spillover of atomic hydrogen from Ni interacts with C(a) species and sequentially hydrogenates carbon until the product methane desorbs.

the Ni/MSN catalyst was revealed after reduction under H_2 at 673 K. The introduction of gaseous carbon dioxide, followed by heating, resulted in the formation of electrons where some of the oxygen vacancies were filled by the adsorption of oxygen from gaseous carbon dioxide. This led to a reduction in the ESR signal at $g = 1.99$ by 24% from 323 to 473 K, as shown in Fig. 7A. The carbon dioxide preadsorbed sample was then heated in the presence hydrogen (Fig. 7B). The ESR signal at $g = 1.99$ was slightly decreased by 17% after increasing the temperature from 323 to 473 K. This indicates that some of the oxygen vacancies were filled with electrons, which may have originated from hydrogen spillover at Ni sites. The discrepancy in the percent decrease, in which the latter adsorption ($CO_2 + H_2$) was lower than the former adsorption (CO_2), was probably due to the formation of methane on the surface of the Ni/MSN catalyst.

The presence of oxygen vacancies in Ni/MSN is necessary to explain the formation of surface carbon species, C(a). It is possible that a C(a) species could interact directly with an oxygen vacancy in MSN. This possibility is supported by the IR observations during pyrrole adsorption (Fig. 3). The basicity (basic oxygen) of MSN is higher than that of Ni/MSN, since the introduction of Ni decreased the population of basic oxygen in MSN. This means that the role of MSN is to adsorb CO_2 as a C(a) species. Albeit the nature of basic oxygen and its correlation to the oxygen vacancies are still under debate, the basic oxygen in the framework may exhibits the oxygen vacancy's character. This was also discussed by recent researcher on zinc oxide system which concluded that the basic sites of zinc oxide were increased with the increased of electronic density on Zn^{2+}–O^{2-} sites. The electronic density was induced by the delocalization of the electrons released through the formation of oxygen vacancies [70]. In addition, the study on the correlation between basic sites and oxygen vacancy is still under study by our group.

The role of Ni sites in MSN may be to dissociate hydrogen to form atomic hydrogen, in which atomic hydrogen facilitates the formation of methane. As shown in Fig. 8, hydrogen will reacts with surface oxygen to produce water and form oxygen vacancies, which will activate additional CO_2 to fill the vacancies and produce CO. It is suggested that the alternative product, CO, is likely produced as an intermediate during methanation. The stability of the CO moiety on the catalyst will determine whether or not the CO will desorb or progress to further reduction. CO dissociation is thought to be the rate determining step for the remaining reduction steps. The pathway to further dissociate CO does not compete significantly with CO desorption. Utilization of H_2 is low since the formation of CO requires only one H_2 while that of methanation requires four.

The interaction of carbonate species with oxygen vacancies in CeO_2 was studied by Goguet et al., in which the adsorbed CO_2 mostly reacted with CeO_2 rather than metal sites [71]. The effect of hydrogen on the ESR signal was similar to the results observed for MoO_3–ZrO_2 [67], Ir/Pt-HZSM5 [68], Pt/HY [69] and catalysts, in which heating the catalysts in the presence of hydrogen partially eliminated the ESR signal assigned to trapped electrons or unpaired electrons in oxygen vacancies that had localized on metal cations (electron-deficient metal cations), representing the formation of electrons via a hydrogen spillover phenomenon. The role of Ni in this study is also supported by Swalus et al. who studied CO_2 methanation over Rh/γ-Al_2O_3 mixed with Ni/activated carbon catalysts [16]. They observed that no CO_2 adsorption occurred on pure activated carbon or on the 1 wt% Ni/activated carbon catalyst. Meanwhile, H_2 was easily adsorbed on the 1 wt% Ni/activated carbon catalyst. Similar to metallic Ni, metallic Pd in the Pd–Mg/SiO_2 system also provided atomic hydrogen spillover to hydrogenate the carbonate and to form methane [17].

3.3.3. *Catalytic stability testing*

The stability test of all Ni catalysts at 573 K was conducted for 200 h where the rate formation of CH_4 are plotted as a function of time-on-stream. As shown in Fig. 9, with time on stream increases, the rate formation of CH_4 of Ni/MCM-41, Ni/HY, Ni/SiO_2 and Ni/γ-Al_2O_3 catalysts decrease slightly, however, the rate formation of CH_4 of Ni/MSN catalyst shows no obvious decrease. The percent decrease of the rate formation of CH_4 for Ni/MCM-41, Ni/HY, Ni/SiO_2 and Ni/γ-Al_2O_3 is 3.4%, 9.0%, 10.6% and 26.6%, respectively. The presence of coke deposition on active sites is known for catalyst deactivation. Carbidic carbon can be a precursor for coke that causes deactivation [72,73]. In order to verify the deposition of coke over these catalysts, TGA was performed in a nitrogen-containing atmosphere and the percent of carbon deposition on the catalysts were measured from TGA (Table 2). From the result, no coke content was observed on Ni/MSN catalyst and the highest coke content was observed on Ni/γAl_2O_3 catalyst (9.1%). To sum up, the Ni/MSN catalyst prepared in this work did not show

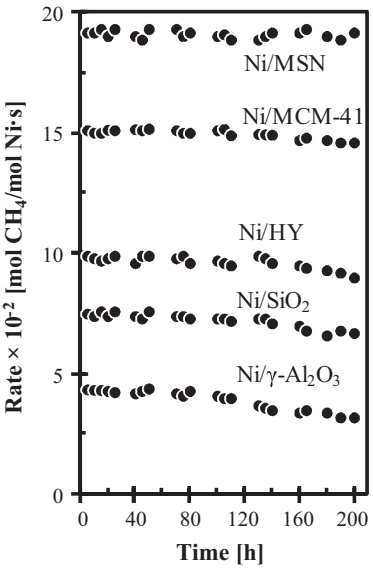

Fig. 9. Long-term stability test of Ni catalysts for CO_2 methanation reaction at a temperature of 573 K, GHSV = 50,000 ml/g h and H_2/CO_2 = 4:1.

any sign of deactivation for the methanation reaction up to 200 h of time-on-stream. Thus, Ni/MSN catalyst is resistant toward coke formation and presented good stabilities under reaction conditions.

4. Conclusions

Mesostructured silica nanoparticles (MSN) and a series of Ni catalysts with different supports (MSN, MCM-41, SiO_2, γ-Al_2O_3 and HY) were prepared by a sol–gel and impregnation method for the methanation of CO_2. The activity of CO_2 methanation followed the order: Ni/MSN > Ni/MCM-41 > Ni/HY > Ni/SiO_2 > Ni/γ-Al_2O_3. This indicates that MSN possesses high potential as a support for Ni catalysts in the methanation reaction. The catalytic performance of Ni/MSN was closely related to the structure of the catalyst, which consisted of both intra- and inter-particle porosity. The presence of interparticle porosity facilitated the transport of reactant and product molecules during the reaction. The higher diffusion of CO_2 in the pores of the Ni/MSN increased overall reaction rates and resulted in a higher increase of the conversion with rising temperature compared to Ni/MCM-41. The internal mass diffusion effect was investigated through Weisz–Prater criterions and the result showed that internal mass transfer resistance was negligible under operating condition and the reaction rate. The high basicity of Ni/MSN catalysts was crucial to the high activity of the reaction and favored an increase in CO_2 adsorption on the catalyst. The presence of defect sites or oxygen vacancies in MSN was responsible for the formation of surface carbon species, while Ni sites dissociate hydrogen into atomic hydrogen. Carbon atoms were then taken by atomic hydrogen for the formation of methane. The Ni/MSN catalyst demonstrated good stability with no deactivation during the entire test period. The results of catalytic tests showed that Ni/MSN is suitable for the CO_2 methanation due to good activity and remarkable resistance to coke formation.

Acknowledgments

This work was supported by Ministry of Science, Technology and Innovation, Malaysia through EScienceFund Research Grant no. 03-01-06-SF0987, MyPhd Scholarship (Muhammad Arif Ab Aziz) from Ministry of Higher Education, Malaysia and the Hitachi Scholarship Foundation for the Gas Chromatograph Instruments Grant.

References

[1] E.E. Benson, C.P. Kubiak, A.J. Sathrum, J.M. Smieja, Chem. Soc. Rev. 38 (2009) 89.
[2] P. Sabatier, J.B. Senderens, Compt. Rend. Acad. Sci. 134 (1902) 514.
[3] K.R. Thampi, J. Kiwi, M. Gratzel, Nature 327 (1987) 506.
[4] C. Galletti, S. Specchia, G. Saracco, V. Specchia, Chem. Eng. Sci. 65 (2010) 590.
[5] D.P. VanderWiel, J.L. Zilka-Marco, Y. Wang, A.Y. Tonkovich, R.S. Wegeng, AIChe 2000, Spring National Meeting, Atlanta, GA, 2000, p. 187.
[6] J. Sehested, K.E. Larsen, A.L. Kustov, A.M. Frey, T. Johannessen, T. Bligaard, M.P. Andersson, J.K. Nørskov, C.H. Christensen, Top. Catal. 45 (2007) 1.
[7] G. Du, S. Lim, Y. Yang, C. Wang, L. Pfefferle, G.L. Haller, J. Catal. 249 (2007) 370.
[8] B. Lu, K. Kawamoto, Fuel 103 (2013) 699.
[9] M. Yamasaki, H. Habazaki, K. Asami, K. Izumiya, K. Hashimoto, Catal. Commun. 7 (2006) 24.
[10] S. Tada, T. Shimizu, H. Kameyama, T. Haneda, R. Kikuchi, Int. J. Hydrogen Energy 37 (2012) 5527.
[11] E. Jwa, S.B. Lee, H.W. Lee, Y.S. Mok, Fuel Process Tech. 108 (2013) 89.
[12] S. Sharma, Z. Hu, P. Zhang, E.W. McFarland, H. Metiu, J. Catal. 278 (2011) 297.
[13] S. Eckle, H.-G. Anfang, R.J. Behm, J. Phys. Chem. C 115 (2011) 1361.
[14] A. Karelovic, P. Ruiz, Appl. Catal., B: Environ. 113–114 (2012) 237.
[15] A. Beuls, C. Swalus, M. Jacquemin, G. Heyen, A. Karelovic, P. Ruiz, Appl. Catal., B: Environ. 113–114 (2012) 2.
[16] C. Swalus, M. Jacquemin, C. Poleunis, P. Bertrand, P. Ruiz, Appl. Catal., B: Environ. 125 (2012) 41.
[17] J.-N. Park, E.W. McFarland, J. Catal. 266 (2009) 92.
[18] T.-W. Kim, P.-W. Chung, V.S.-Y. Lin, Chem. Mater. 22 (2010) 5093.
[19] K.-P. Yu, W.-Y. Yu, M.-C. Kuo, Y.-C. Liou, S.-H. Chien, Appl. Catal., B: Environ. 84 (2008) 112.
[20] C.K. Vance, C.H. Bartholomew, Appl. Catal. 7 (1983) 169.
[21] S. Sokolov, E.V. Kondratenko, M.-M. Pohl, A. Barkschat, U. Rodemerck, Appl. Catal., B: Environ. 113–114 (2012) 19.
[22] I. Rossetti, C. Biffi, C.L. Bianchi, V. Nichele, M. Signoretto, F. Menegazzo, E. Finocchio, G. Ramis, A.D. Michele, Appl. Catal., B: Environ. 117–118 (2012) 384.
[23] V. Nichele, M. Signoretto, F. Menegazzo, A. Gallo, V.D. Santo, G. Cruciani, G. Cerrato, Appl. Catal., B: Environ. 111–112 (2012) 225.
[24] H. Zheng, C. Gao, B. Peng, M. Shu, S. Che, J. Phys. Chem. C 115 (2011) 7230.
[25] Y.-S. Lin, C.L. Haynes, J. Am. Chem. Soc. 132 (2010) 4834.
[26] M. Liong, S. Angelos, E. Choi, K. Patel, J.F. Stoddart, J.I. Zink, J. Mater. Chem. 19 (2009) 6251.
[27] Y. Sakamoto, M. Kaneda, O. Terasaki, D.Y. Zhao, J.M. Kim, G. Stuckyk, H.J. Shin, R. Ryoo, Nature 408 (2000) 449.
[28] J. Dou, H.C. Zheng, J. Am. Chem. Soc. 134 (2012) 16235.
[29] F. Jiao, H. Frei, Angew. Chem. Int. Ed. 48 (2009) 1841.
[30] V. Hulea, D. Brunel, A. Galarneau, K. Philippot, B. Chaudret, P.J. Kooyman, F. Fajula, Microporous Mesoporous Mater. 79 (2005) 185.
[31] A.H. Karim, A.A. Jalil, S. Triwahyono, S.M. Sidik, N.H.N. Kamarudin, R. Jusoh, N.W.C. Jusoh, B.H. Hameed, J. Colloid Interface Sci. 386 (2012) 307.
[32] J.S. Beck, J.C. Vartuli, W.J. Roth, M.E. Leonowicz, C.T. Kresge, K.D. Schmitt, C.T.-W. Chu, D.H. Olson, E.W. Sheppard, S.B. McCullen, J.B. Higgins, J.L. Schlenker, J. Am. Chem. Soc. 114 (1992) 10834.
[33] B.D. Cullity, Elements of X-ray Diffraction, second ed., Addison-Wesley, Reading, MA, 1978.
[34] H. Hattori, Chem. Rev. 95 (1995) 537.
[35] M. Sánchez-Sánchez, T. Blasco, J. Am. Chem. Soc. 124 (2002) 3443.
[36] Z. Liu, J. Zhou, K. Cao, W. Yang, H. Gao, Y. Wang, H. Li, Appl. Catal., B: Environ. 125 (2012) 324.
[37] M. El Doukkali, A. Iriondo, P.L. Arias, J. Requies, I. Gandarías, L. Jalowiecki-Duhamel, F. Dumeignil, Appl. Catal., B: Environ. 125 (2012) 516.
[38] S. Wang, G.Q.M. Lu, Appl. Catal., B: Environ. 16 (1998) 269.
[39] E. Prouzet, F. Cot, G. Nabias, A. Larbot, P. Kooyman, T.J. Pinnavaia, Chem. Mater. 11 (1999) 1498.
[40] H.Y. Kim, H.M. Lee, J.-N. Park, J. Phys. Chem. C 114 (2010) 7128.
[41] V. Cauda, C. Argyo, A. Schlossbauer, T. Bein, J. Mater. Chem. 20 (2010) 4305.
[42] E. Ghedini, F. Menegazzo, M. Signoretto, M. Manzoli, F. Pinna, G. Strukul, J. Catal. 273 (2010) 266.
[43] S.J. Gregg, K.S.W. Sing, Adsorption, Surface Area and Porosity, Academic Press, London, UK, 1982.
[44] P.A. Robles-Dutenhefner, K.A. da Silva Rocha, E.M.B. Sousa, E.V. Gusevskaya, J. Catal. 265 (2009) 72.
[45] K.S.W. Sing, D.H. Everett, R.A.W. Haul, L. Moscou, R.A. Pierotti, J. Rouquerol, T. Siemieniewska, Pure Appl. Chem. 57 (1985) 603.
[46] H. Förster, H. Fuess, E. Geidel, B. Hunger, H. Jobic, C. Kirschhock, O. Klepel, K. Krause, Phys. Chem. Chem. Phys. 1 (1999) 593.
[47] D. Murphy, P. Massiani, R. Franck, D. Barthomeuf, J. Phys. Chem. 100 (1996) 6731.
[48] P.O. Scokart, P.G. Rouxhet, J.C.S. Faraday I 76 (1980) 1476.
[49] C. Binet, A. Jadi, J. Lamotte, J.C. Lavalley, J. Chem. Soc., Faraday Trans. 92 (1996) 123.
[50] D.C.D. da Silva, S. Letichevsky, L.E.P. Borges, L.G. Appel, Int. J. Hydrogen Energy 37 (2012) 8923.
[51] H. Tsuji, F. Yagi, H. Hattori, Chem. Lett. 20 (1991) 1881.
[52] F. Solymosi, A. Erdohelyi, M. Kocsis, J. Chem. Soc., Faraday Trans. I 77 (1981) 1003.

[53] T. Abe, M. Tanizawa, K. Watanabe, A. Taguchi, Energy Environ. Sci. 2 (2009) 315.
[54] N. Perkas, G. Amirian, Z. Zhong, J. Teo, Y. Gofer, A. Gedanken, Catal. Lett. 130 (2009) 455.
[55] S. Takenaka, T. Shimizu, K. Otsuka, Int. J. Hydrogen Energy 29 (2004) 1065.
[56] F. Solymosi, A. Erdöhelyi, T. Bánsági, J. Catal. 68 (1981) 371.
[57] D.E. Peebles, D.W. Goodman, J.M. White, J. Phys. Chem. 87 (1983) 4378.
[58] T. Inui, M. Funabiki, Chem. Lett. 7 (1978) 251.
[59] T. Van Herwijnen, H. Van Doesburg, W.A. De Jong, J. Catal. 28 (1973) 391.
[60] A. Wang, Y.-P. Hsieh, Y.-F. Chen, C.-Y. Mou, J. Catal. 237 (2006) 197.
[61] Y.P. Khitev, I.I. Ivanova, Y.G. Kolyagin, O.A. Ponomareva, Appl. Catal., A: Gen. 441–442 (2012) 124.
[62] G. Seo, F.E. Massoth, AIChE J. 31 (1985) 494.
[63] H.S. Fogler, Elements of Chemical Reaction Engineering, second ed., Prentice-Hall, Englewood Cliffs, NJ, 1992.
[64] V. Zeleňák, A. Zeleňáková, J. Kováč, Colloids Surf., A 357 (2010) 97.
[65] R.S. Ningthoujam, D. Lahiri, V. Sudarsan, H.K. Poswal, S.K. Kulshreshtha, S.M. Sharma, B. Bhushan, M.D. Sastry, Mater. Res. Bull. 42 (2007) 1293.
[66] X. Pan, M.-Q. Yang, X. Fu, N. Zhang, Y.-J. Xu, Nanoscale 5 (2013) 3601.
[67] N.N. Ruslan, S. Triwahyono, A.A. Jalil, S.N. Timmiati, N.H.R. Annuar, Appl. Catal., A: Gen. 413–414 (2012) 176.
[68] H.D. Setiabudi, A.A. Jalil, S. Triwahyono, J. Catal. 294 (2012) 128.
[69] M.A.A. Aziz, N.H.N. Kamarudin, H.D. Setiabudi, H. Hamdan, A.A. Jalil, S. Triwahyono, J. Nat. Gas Chem. 21 (2012) 29.
[70] C. Drouilly, J.-M. Krafft, F. Averseng, H. Lauron-Pernot, D. Bazer-Bachi, C. Chizallet, V. Lecocq, G. Costentin, Appl. Catal., A: Gen. 453 (2013) 121.
[71] A. Goguet, F.C. Meunier, D. Tibiletti, J.P. Breen, R. Burch, J. Phys. Chem. B 108 (2004) 20240.
[72] J. Yang, X. Wang, L. Li, K. Shen, X. Lu, W. Ding, Appl. Catal., B: Environ. 96 (2010) 232.
[73] S. Lee, G. Keskar, C. Liu, W.R. Schwartz, C.S. McEnally, J.-Y. Kim, L.D. Pfefferle, G.L. Haller, Appl. Catal., B: Environ. 111–112 (2012) 157.